Bioactive Materials 19 (2023) 115–126

Contents lists available at ScienceDirect

Bioactive Materials

journal homepage: www.keaipublishing.com/en/journals/bioactive-materials

Reactive oxygen species (ROS)-responsive size-reducible nanoassemblies for deeper atherosclerotic plaque penetration and enhanced macrophage-targeted drug delivery

Jianhua He [a,1], Wenli Zhang [a,1], Xiaoju Zhou [a], Fengfei Xu [a], Jiahui Zou [a], Qiqi Zhang [a], Yi Zhao [b], Hongliang He [c], Hu Yang [d,*], Jianping Liu [a,**]

[a] Department of Pharmaceutics, China Pharmaceutical University, Nanjing, Jiangsu, 210009, PR China
[b] School of Biomedical Engineering, Sun Yat-sen University, Shenzhen, 518107, PR China
[c] State Key Laboratory of Bioelectronics, Jiangsu Key Laboratory for Biomaterials and Devices, School of Biological Science and Medical Engineering, Southeast University, Nanjing, 210096, PR China
[d] Linda and Bipin Doshi Department of Chemical and Biochemical Engineering, Missouri University of Science and Technology, Rolla, MO, 65401, United States

ARTICLE INFO

Keywords:
Atherosclerosis
Macrophage
Reactive oxygen species
Size-reducible nanoassemblies
Recombinant high-density lipoprotein

ABSTRACT

Nanoparticle-based therapeutics represent potential strategies for treating atherosclerosis; however, the complex plaque microenvironment poses a barrier for nanoparticles to target the dysfunctional cells. Here, we report reactive oxygen species (ROS)-responsive and size-reducible nanoassemblies, formed by multivalent host-guest interactions between β-cyclodextrins (β-CD)-anchored discoidal recombinant high-density lipoprotein (NP^3_{ST}) and hyaluronic acid-ferrocene (HA-Fc) conjugates. The HA-Fc/NP^3_{ST} nanoassemblies have extended blood circulation time, specifically accumulate in atherosclerotic plaque mediated by the HA receptors CD44 highly expressed in injured endothelium, rapidly disassemble in response to excess ROS in the intimal and release smaller NP^3_{ST}, allowing for further plaque penetration, macrophage-targeted cholesterol efflux and drug delivery. *In vivo* pharmacodynamicses in atherosclerotic mice shows that HA-Fc/NP^3_{ST} reduces plaque size by 53%, plaque lipid deposition by 63%, plaque macrophage content by 62% and local inflammatory factor level by 64% compared to the saline group. Meanwhile, HA-Fc/NP^3_{ST} alleviates systemic inflammation characterized by reduced serum inflammatory factor levels. Collectively, HA-Fc/NP^3_{ST} nanoassemblies with ROS-responsive and size-reducible properties exhibit a deeper penetration in atherosclerotic plaque and enhanced macrophage targeting ability, thus exerting effective cholesterol efflux and drug delivery for atherosclerosis therapy.

1. Introduction

Atherosclerosis is a chronic inflammatory disease, the underlying cause of many life-threatening cardiovascular events [1–3]. Intimal macrophages play a critical role in atherosclerotic progression [4–6]. At early stages, monocytes are recruited to the intima and differentiate into macrophages. Within the intima, those macrophages engulf excessive amounts of oxidized lipoprotein particles and turn into pathological macrophage/foam cells. Foam cells secrete inflammatory factors to induce a maladaptive inflammatory response, eventually leading to the destabilization of atherosclerotic plaques. Delivering drugs to intimal macrophage/foam cells to suppress plaque inflammation is a potential intervention strategy for atherosclerosis therapy [7–9]. Nanoparticles have been widely utilized as drug and gene carriers for atherosclerosis therapy [10–12]. Nanoparticles must penetrate a thick fibrous cap—mainly composed of vascular smooth muscle cells and collagenous fibers—through leaky vasculature and subsequent inflammatory cell-mediated sequestration (ELVIS) effect [13,14] before they reach pathological macrophage/foam cells [15,16]. Although particles in the range of 100–200 nm typically have prolonged circulation in the blood,

Peer review under responsibility of KeAi Communications Co., Ltd.
* Corresponding author.
** Corresponding author.
E-mail addresses: huyang@mst.edu (H. Yang), jianpingliu1293@163.com (J. Liu).
[1] These authors contributed equally to this work.

https://doi.org/10.1016/j.bioactmat.2022.03.041
Received 26 January 2022; Received in revised form 22 March 2022; Accepted 29 March 2022

their penetration in atherosclerotic plaque is limited [17,18]. Instead, nanoparticles of smaller size (sub 40 nm) can effectively penetrate plaque tissue and reach intimal macrophage/foam cells [19], but their plaque accumulation is insufficient due to short circulation time [18,20]. To effectively end up in atherosclerotic lesions, nanoparticles are desired to have extended blood circulation and deep atherosclerotic plaque penetration.

In atherosclerotic plaque, excess reactive oxygen species (ROS) are produced by pathologic resident cells [21–23]. Although ROS-responsive materials have been developed to utilize oxidative microenvironment for biomedical applications, including atherosclerosis therapy [24–30], using ROS stimulus to design a smart delivery system for more efficient delivery of drugs to atherosclerotic plaques has not been attempted before. In this study, we developed a ROS-responsive size-reducible nanocarrier on the basis of multivalent host-guest interactions of β-cyclodextrins (β-CD)/ferrocene (Fc) for targeted treatment of atherosclerosis (Scheme 1). In this delivery system, simvastatin (ST) was selected as a model statin drug to suppress plaque inflammation and promote cholesterol efflux [31–33]. β-CD-anchored discoidal recombinant high-density lipoprotein (rHDL), termed as NP^3_{ST}, was utilized as a core as it was shown to possess not only deep plaque penetration property by virtue of its small size but also plaque targeting and cholesterol removal ability [34,35]. Fc was grafted onto hyaluronic acid (HA), and the resulting HA-Fc conjugates were utilized to crosslink NP^3_{ST} through multivalent host-guest interactions between β-CD/Fc to form ROS-responsive nanoassemblies (HA-Fc/NP^3_{ST}) [36,37]. We engineered the particles of nanoassemblies to have the size in the range of 100–200 nm in order to have extended circulation time in the blood. HA was expected to guide the nanoparticles to accumulate in the plaque lesions area by targeting the CD44 receptors that are highly expressed in endothelial cells of plaque lesions [38–40]. Upon entering the plaque intima, the hydrophobic Fc was expected to be oxidized into hydrophilic ferrocenium ion (Fc+) under the action of excess ROS [41,42], leading to disintegration between β-CD/Fc and the disassembly of HA-Fc/NP^3_{ST}. The released NP^3_{ST} was expected to play an essential role in atherosclerosis by penetrating through plaque, targeting the macrophage/foam cells, and mediating cholesterol efflux. We characterized the structure, properties and functions of HA-Fc/NP^3_{ST} both *in vitro* and *in vivo*. We tested and confirmed the delivery efficiency and efficacy of HA-Fc/NP^3_{ST} in an animal model of atherosclerosis.

2. Materials and methods

2.1. Materials

Sodium hyaluronic acid (HA, molecular weight 150 kDa) was purchased from Freda Biochem Co., Ltd. (Shandong, China). Amantadine hydrochloride, coumarin 6 (C6, Ex/Em, 465/502) and Hoechst 33342 (Ex/Em, 346/460) were obtained from Aladdin (Shanghai, China). Ferrocenylmethylamine hydrochloride (Fc-NH_2) was purchased from Xuzhou Guanrong Pharmaceutical&Chemical Co. Ltd. (Jiangsu, China). Soybean phospholipid (SPC) was purchased from A.V.T. Pharmaceutical Co. Ltd. (Shanghai, China). NBD-cholesterol (Ex/Em, 472/540) was obtained from Cayman Chemical (USA). Simvastatin (ST) was kindly donated by Shangyu Jingxin Pharmacy Company (Shaoxing, China). β-cyclodextrin (β-CD) was obtained from Zhiyuan Biotechnology Co., Ltd (Binzhou, China). Dulbecco's modified Eagle's medium (DMEM) and fetal bovine serum (FBS) were purchased from Wisent (Nanjing, China). 3-(4,5-dimethylthiazol-2-yl)-2,5-diphenyltetrazolium bromide (MTT), penicillin, streptomycin and oil red O were purchased from Sigma-Aldrich (USA). Oxidized low-density lipoprotein (oxLDL) was obtained from Yiyuan Biotech. Co., Ltd (Guangzhou, China). Rhodamine 123 (Rho123, Ex/Em, 490/524), rhodamine isothiocyanate (RITC, Ex/Em, 490/575) and 1,1′-dioctadecyl-3,3,3′,3′-tetramethylindotricarbocyanine iodide (DiR, Ex/Em, 748/780) were purchased from Nanjing Senbeijia Biological Technology Co., Ltd (Jiangsu, China). D-

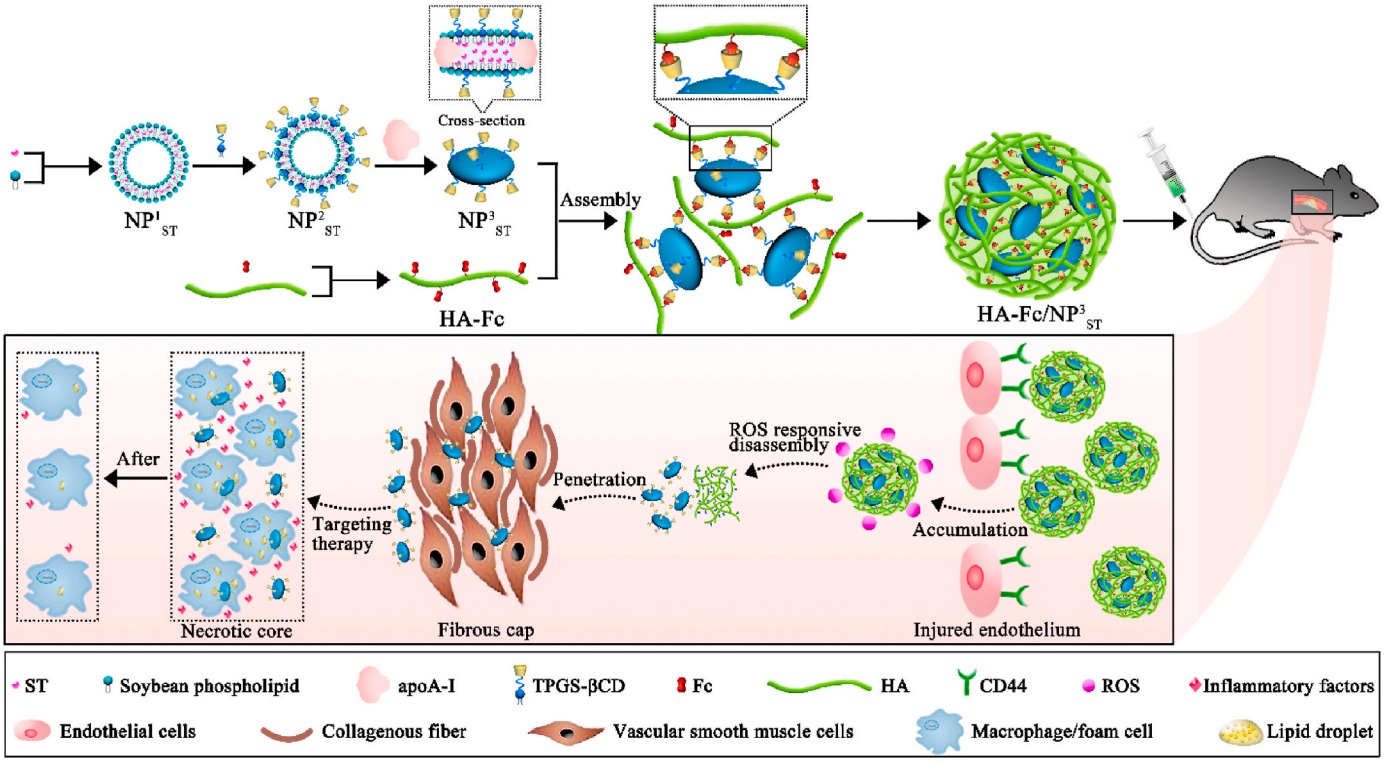

Scheme 1. Illustration of the assembly of ROS-responsive size-reducible HA-Fc/NP^3_{ST} nanoassemblies and their desired performance *in vivo*. Small-sized NP^3_{ST} is crosslinked by HA-Fc conjugates to large-sized HA-Fc/NP^3_{ST} nanoassemblies through multivalent host-guest interactions between β-CD/Fc. After accumulating in atherosclerotic plaque mediated by the HA-CD44 recognition, HA-Fc/NP^3_{ST} rapidly disassembles caused by excess ROS in the intima and releases smaller NP^3_{ST}, allowing for further plaque penetration to regress atherosclerotic plaque via macrophage-targeted cholesterol efflux and drug delivery.

α-tocopheryl polyethylene glycol 1000 succinate (TPGS)-block-β-CD conjugates (TPGS-βCD) was synthesized by our lab [34]. The apolipoprotein A-I (apoA-I; 97% purity) was isolated from the industrial waste during the production of albumin in our lab [43]. Lecithin cholesterol acyl transferase (LCAT) was isolated from the human plasma by using agarose gel chromatography from human plasma [44]. Methanol and acetonitrile of chromatographic grade were used for HPLC analysis. All other reagents were of analytical grade.

2.2. Synthesis and characterization of HA-Fc conjugates

HA-Fc conjugates were synthesized by grafting Fc-NH_2 onto the HA backbone through amidation reaction [45]. The synthesized HA-Fc conjugates were characterized by using ^{1}H-NMR analysis in D_2O at 500 MHz (Bruker AVANCE AV-500, Germany). The grafting degree (*GD*) of Fc in HA-Fc, defined as the number of Fc per 100 sugar residues of HA-Fc, was calculated by iron content (*P*, %) of the product shown in equation (1). The *P* was measured by Inductively Coupled Plasma Optical Emission Spectrometer (ICP-OES, PerkinElmer Optima8000, USA) under the conditions shown in Table S1. Besides, amantadine (Am) was utilized as a surrogate of Fc-NH_2 to synthesize HA-Am. The *GD* of Am in HA-Am conjugates was obtained from the ^{1}H-NMR spectrums by comparing the integrals of signals at δ 1.65–1.85 (peak III) and δ 2.10 (peak 3) in Fig. S1 [46].

$$GD = \frac{379 \times P}{56 - 197 \times P} \quad (1)$$

2.3. Preparation of nanoparticles

To prepare NP^3_{ST}, ST-loaded liposome (NP^1_{ST}) was prepared by using ethanol injection method [35]. Then TPGS-block-β-CD (TPGS-βCD) conjugates were inserted into NP^1_{ST} via post-insertion method in water bath under a rotation rate of 100 rpm at 37 °C for 5 h to anchor β-CD on the surface of NP^1_{ST} (NP^2_{ST}). Finally, NP^3_{ST} was obtained by incubating NP^2_{ST} with apoA-I (6 mg/mL) in the presence of sodium cholate under stirring at room temperature for 8 h [47].

HA-Fc/NP^3_{ST} was prepared by incubating HA-Fc with NP^3_{ST}. Briefly, HA-Fc was dissolved in Tris-HCl buffer (0.01 M, pH 8.0) and then dropwise added into NP^3_{ST} solution under stirring at room temperature for 8 h (molar ratio of Fc/β-CD was 1:1). After that, the mixture was incubated in an ultrasonic bath at room temperature for 3 h. All the operation was processed in dark. Finally, the mixture was sterile-filtered through 0.22 μm millipore filter, and HA-Fc/NP^3_{ST} was obtained. Besides, HA-Am/NP^3_{ST}, served as ROS-unresponsive control nanoassemblies, was prepared by incubating HA-Am with NP^3_{ST} under the same operations.

2.4. Particle size, zeta potential, entrapment efficiency (EE), and drug loading (DL) measurements

The nanoparticles' particle size and zeta potential were measured by dynamic light scattering (DLS) (Brookhaven Instruments, U.S.A) at 25 °C. The *EE* and *DL* of drug-loaded nanoparticles were quantified by using the mini-column centrifugation method [35,48].

2.5. Stability assessments

The storage stability, dilution stability and LCAT resistance capacity of the nanoparticles were assessed by measuring the change of particle size and *EE*. Briefly, the nanoparticles were incubated in Tris-HCl buffer at 4 °C for 14 days, diluted by 50 times with Tris-HCl buffer and incubated with 4.67 μg/mL LCAT (mimicking plasma LCAT level in the examined subjects [49]) for 2 h and 24 h, respectively. The changes of particle size and *EE* were measured. The drug leakage ratio was expressed as the percentage of *EE* reduction after storage relative to the *EE* before storage [50].

2.6. Fluorescence resonance energy transfer (FRET) assay

Nanoassemblies between HA-Fc and NP^3_{ST} was verified by FRET analysis. Rho 123 and RITC, used as FRET pairs, were conjugated onto HA-Fc and apoA-I, respectively [51]. Then, Rho 123-labeled HA-Fc and/or RITC-labeled apoA-I were utilized to prepare the fluorescence-labeled HA-Fc/NP^3_{ST}. The excitation and emission wavelengths of these channels were listed in Table S2, and the fluorescence intensities were measured by fluorescence spectrophotometer (RF-5301PC, Shimadzu, Japan). FRET index was calculated by using equation (2) [52].

$$FRET\ index = \frac{F_b}{D_b} - \frac{F_d}{D_d} \quad (2)$$

Where F_b and D_b mean the fluorescence intensity of dual-labeled nanoassemblies in the channel F and D, F_d and D_d mean the fluorescence intensity of Rho 123-labeled nanoassemblies in the channel F and D.

2.7. ROS-responsiveness assessment

The H_2O_2-triggered oxidation of Fc was first assessed as described in Supporting Information. The ROS-responsiveness of the HA-Fc/NP^3_{ST} was then evaluated by using the FRET method. Briely, the dual fluorescence-labeled Rho123-HA-Fc/NP^3_{ST}-RITC was incubated in Tris-HCl buffer supplemented with 0.02 mM of H_2O_2 (mimicking the ROS concentration in normal tissue [53]) or 1 mM of H_2O_2 (mimicking the ROS concentration in atherosclerotic plaque [54]). The FRET index was determined at 0, 1, 2, 4 and 8 h post-incubation. Besides, ROS-responsiveness of HA-Am/NP^3_{ST} was evaluated. Furthermore, the morphologies of HA-Fc/NP^3_{ST} before and after treatment by 1 mM of H_2O_2 for 2 h were imaged by transmission electron microscopy (TEM) (H-7650, Hitachi High-Technologies Corporation, Japan) [35]. Finally, nanoparticles were mixed in Tris-HCl buffer supplemented with 1 mM H_2O_2. After incubation for 0, 1, 2, 4 and 8 h, the mixture were diluted by 20 times, and particle size and zeta potential were determined.

2.8. Verification of multivalent host-guest interaction

Multivalent host-guest interaction property of the HA-Fc/NP^3_{ST} was evaluated by FRET method. The dual fluorescence-labeled Rho123-HA-Fc/NP^3_{ST}-RITC was incubated in Tris-HCl buffer supplemented with 0, 1, 5 or 50 equivs of free β-CD. The FRET index was determined at 0, 1, 3, and 12 h post-incubation.

2.9. In vitro drug release studies

Dialysis method was utilized to study *in vitro* release kinetics of ST. Briefly, the nanoparticle was mixed with 1 mM H_2O_2, and 3 mL of the mixture was loaded into dialysis tube (molecular weight cutoff at 3500 Da). The dialysis tube was immersed in the medium consisting of 100 mL PBS (0.01 M, pH 7.4) supplemented with 1 mM H_2O_2 as well as 0.5% sodium dodecyl sulfonate (SDS). The dialysis tube was incubated at 37 °C water bath under a rotation rate of 100 rpm for 120 h. The released ST was sampled from the release medium at pre-determined time points and measured by using HPLC [35]. Drug release profiles in the absence of H_2O_2 were determined for comparison.

2.10. Cell viability assay

Murine aortic endothelial cells (MAECs) and RAW 264.7 cells were cultured in DMEM supplemented with 10% FBS, 100 U/mL penicillin and 100 μg/mL streptomycin sulfate at 37 °C and 5% CO_2. The

cytotoxicities of the formulated nanoparticles on MAECs and RAW 264.7 cells were assessed by using MTT method [35].

2.11. Construction of cell models

MAECs (5.0×10^4) were seeded on a Transwell polyester membrane cell culture insert in 24-well plate (pore size 0.4 μm, diameter 6.5 mm, Corning Incorporated, Corning, NY, USA). The transendothelial electrical resistance (TEER) values of the endothelium monolayer were measured by using an electrical resistance meter (Millicell®-Electrical Resistance System, Millipore, USA), and a continuous endothelium monolayer formed until the cell monolayer exhibited a steady TEER value [55,56]. Macrophage spheroids were prepared with RAW 264.7 cells using the hanging-drop/agarose method [57,58]. In addition, macrophage monolayer was obtained by seeding RAW 264.7 cells in the lower chamber of Transwell.

To construct injured endothelium-macrophage spheroid model, the obtained macrophage spheroids were handpicked and translocated to the lower chamber of Transwell. Then tumor necrosis factor-α (TNF-α) (10 ng/mL) was added to the upper chamber to damage the intact cell monolayer. In order to evaluate the change of the endothelium cell monolayer, TEER values were monitored and the expression of CD44 on MAECs was quantified using a flow cytometer (MACSQuant, Miltenyi Biotec, Gladbach, Germany). In addition, an injured endothelium-macrophage monolayer model was constructed via replacing the macrophage spheroids with macrophage monolayer [51].

2.12. Cellular drug uptake study

In the injured endothelium-macrophage monolayer model and injured endothelium-macrophage spheroid model, the culture medium in the upper chamber was replaced with fresh medium containing nanoparticles and the culture medium in the lower chamber was replaced with fresh medium supplemented with 1 mM of H_2O_2. After incubation at 37 °C for different lengths of time, the culture medium and cells in the lower chamber were collected for quantification of the drug content by using HPLC and protein content via BCA assay (Beyotime Institute of Biotechnology, China), respectively. The amount of drug uptake was indirectly determined by subtracting the amount of drug in the culture medium from the total amount of the added drugs. The amount of cellular drug uptake was normalized based on the cell protein content of each group and expressed as μg mg^{-1} protein [35,47].

2.13. Transendothelial investigation

Transport of nanoparticles across the endothelium monolayer was evaluated by measuring the apparent permeability coefficient (Papp, cm/s) of ST [51,59]. The effect of free HA or sodium azide on ST permeation was investigated via pretreatment of the endothelial cells with free HA (10 mg/mL) for 2 h or sodium azide (1 mg/mL) for 1 h. In addition, permeation of nanoparticles across the continuous endothelial monolayer was determined.

2.14. Penetration study

Penetration of nanoparticles in the macrophage spheroids was evaluated by using confocal laser scanning microscope (CLSM). Briefly, the obtained macrophage spheroids were handpicked and translocated to 15 mm glass-bottom dishes. Next, hydrophobic fluorescent dye C6 was loaded into nanoparticles as a surrogate of ST, and the macrophage spheroids were treated with 1 mL of C6-loaded nanoparticles supplemented with 1 mM of H_2O_2 for 8 h. After that, the macrophage spheroids were rinsed with PBS thrice and imaged by CLSM (LSM700, Carl Zeiss, Germany) using Z-stack scanning from the top of the macrophage spheroid to the equatorial plane [60]. The fluorescence intensity in the center of macrophage spheroids at equatorial plane was analyzed by Image-Pro Plus 6 to represent the penetration ability of nanoparticles [61]. Besides, penetration of nanoparticles in macrophage spheroids was evaluated in the absence of H_2O_2.

2.15. Macrophage targeting studies

Macrophage targeting behavior of nanoparticles was assessed using the injured endothelium-macrophage monolayer model. The C6-loaded nanoparticles were added to the upper chamber and the medium in the lower chamber was changed to fresh medium supplemented with 1 mM of H_2O_2. After incubation for 8 h, the fluorescence intensities of C6 in macrophages were determined by flow cytometry. To investigate the influence factors in macrophage targeting behavior of nanoparticles, the overexpressed CD44 on MAECs were blocked by pretreatment with free HA (10 mg/mL) for 2 h [51], the medium in the lower chamber was changed to the fresh medium without H_2O_2 or the overexpressed SR-BI on macrophages were blocked by pretreatment with free apoA-I (50 mg/mL) for 2 h [62]. For fluorescent microscopic analyses, macrophages were cultured on the glass coverslips in the lower chamber of transwell. After incubation, the macrophages were rinsed with PBS thrice, counterstained with Hoechst 33342 (10 mg/mL) for 15 min and finally imaged under CLSM.

2.16. Cholesterol efflux assay

Cholesterol efflux assay was investigated in the injured endothelium-macrophage monolayer model. The RAW 264.7 cells in the lower chamber of Transwell were incubated with oxLDL (60 μg/mL) and NBD-cholesterol (5 μM) for 24 h. Then, the cells were washed and treated with fresh medium supplemented with 1 mM of H_2O_2. In the meantime, nanoparticles were added to the upper chamber and incubated for 24 h. Finally, the amount of NBD-cholesterol in the media and macrophages lysates were quantified by a microplate reader at an excitation of 469 nm and an emission wavelength of 537 nm. Cholesterol efflux (%) was expressed as the percentage of fluorescence intensity in the media relative to the total fluorescence intensity in the media and cell lysates [63]. The effects of nanoparticles on the cholesterol content, permeability and fluidity of cell membrane of macrophages in the injured endothelium-macrophage monolayer model were evaluated [35]. RAW 264.7 cells in the lower chamber of Transwell treated with DMEM alone, or oxLDL alone were tested as control groups.

2.17. Intracellular lipid deposition

Intracellular lipid deposition was assessed in the injured endothelium-macrophage monolayer model. The RAW 264.7 cells in the lower chamber of Transwell were incubated with oxLDL (60 μg/mL) for 24 h. Then, the cells were washed and treated with fresh medium supplemented with 1 mM of H_2O_2. In the meantime, nanoparticles were added to the upper chamber and incubation for 24 h. Finally, the intracellular lipid deposition in the macrophages was imaged under inverted fluorescence microscope (IX53, Olympus, Japan) and the positive staining area (%) was quantified by Image-Pro Plus 6 [47]. RAW 264.7 cells in the lower chamber of Transwell treated with DMEM alone or oxLDL alone were tested as control groups.

2.18. Macrophage phenotypic analysis

RAW 264.7 cells seeded in the lower chamber of Transwell were incubated with oxLDL (60 μg/mL) for 24 h. Then, the cells were treated with fresh DMEM medium supplemented with 1 mM of H_2O_2. In the meantime, nanoparticles were added to the upper chamber. The cells were incubated for 24 h and then collected for macrophage phenotypic analysis [34]. RAW 264.7 cells in the lower chamber of Transwell treated with DMEM alone or oxLDL alone were tested as control groups.

2.19. Inflammatory cytokine inhibition assays

RAW 264.7 cells in the lower chamber of Transwell were incubated with oxLDL (60 μg/mL) for 24 h. Then, the cells were treated with fresh medium supplemented with 1 mM of H_2O_2. In the meantime, nanoparticles were added to the upper chamber and incubation for 24 h. After that, the medium in the lower chamber was centrifuged at 12000 rpm for 10 min at 4 °C. The supernatants were collected to measure the concentrations of interleukin-6 (IL-6), TNF-α and chemokine ligand 2 (CCL2) using ELISA kit (Dakewe Biotech Co., Ltd, China), respectively. RAW 264.7 cells in the lower chamber of Transwell treated with oxLDL alone were tested as a control group.

2.20. Atherosclerosis model

The animal experiments in this study were carried out in accordance with the National Institute of Health Guide for the Care and Use of Laboratory Animals. The protocol was approved by Institutional Animal Care and Use Committee of China Pharmaceutical University. Male wild-type C57BL/6 mice (6 weeks) were purchased from Qinglong Mountain Animal center (Nanjing, China). Male apoE-deficient mice (5 weeks) were obtained from the Model Animal Research Center of Nanjing University (Nanjing, China) and utilized to develop an atherosclerosis model via feeding a high-cholesterol diet (21% fat and 0.15% cholesterol) for 16 weeks [51,64].

2.21. Pharmacokinetic study in wild-type C57BL/6 mice

Hydrophobic fluorescent dye DiR was loaded into nanoparticles as a surrogate of ST. The wild-type C57BL/6 mice were randomly divided into 4 groups of three (n = 3) and injected with DiR-labeled Nanoparticles via tail vein. At fixed time points, an equal volume of blood samples was collected into 96-well black plates. An IVIS system (FX PRO, Kodak, USA) was utilized to measure the fluorescence intensity of blood samples at 0, 1, 2, 4, 8, 12 and 24 h post-injection.

2.22. Tissue distribution in atherosclerotic mice

The atherosclerotic mice were randomly divided into 4 groups of three (n = 3) and injected with DiR-labeled nanoparticles via tail vein. After injection for 4 h or 24 h, the mice were sacrificed. Major organs (heart, liver, spleen, lung, kidney) and aortic trees were collected and then imaged under an IVIS system using 720 nm excitation and 790 nm emission filters [64].

2.23. Plaque penetration and macrophage colocalization in atherosclerotic mice

The atherosclerotic mice were randomly divided into 2 groups of three (n = 3) and injected with DiR-labeled nanoparticles via tail vein. At 4 h after injection, the mice were sacrificed. The aortic roots were collected and 8 μm thick paraffin sections were prepared, which were further processed with CD31 [65] or CD68 [66] immunostaining. Finally, the slides were observed by CLSM.

2.24. Pharmacodynamics study in atherosclerotic mice

The atherosclerotic mice were randomly divided into 5 groups of six (n = 6). All groups were treated with two injections per week (3–4 days apart) via tail vein for 12 weeks: (i) saline, (ii) saline, (iii) NP^3_{ST}, (iv) HA-Am/NP^3_{ST}, (v) HA-Fc/NP^3_{ST}. Besides, the second group received ST orally per day during the treatment. The ST dose in each group was 15 mg/kg. Notably, the mice were fed with high-cholesterol diet during the therapeutic period. Finally, the mice were euthanized, the serum levels of inflammatory factors (IL-6, TNF-α and CCL2) were determined by using ELISA kit, and the aortic roots were collected for hematoxylin and eosin (H&E) staining, oil red O staining, CD68 immunostaining and CCL2 immunostaining [51]. Microscopic images of the aortic root sections were digitized and quantified with Image Pro Plus 6.0 software.

2.25. Safety study in atherosclerotic mice

The atherosclerotic mice were randomly divided into 2 groups of six (n = 6), which received saline or HA-Fc/NP^3_{ST} (15 mg/kg ST) two injections per week (3–4 days apart) via tail vein for 12 weeks. After that, blood samples were gathered for biochemical analysis of alanine aminotransferase (ALT), aspartate transaminase (AST) and alkaline phosphatase (ALP) via ELISA kit (Dakewe, China). Besides, main tissues (heart, liver, spleen, lung, kidney) were collected for H&E staining and imaged under an inverted fluorescence microscope.

2.26. Statistical analysis

All values were expressed as mean ± standard deviation (SD). Statistical analysis was performed with mann whitney u test or One-way ANOVA by SPSS 19.0 (IBM Corporation, USA). Significance was reported as $^*p < 0.05$, $^{**}p < 0.01$ or $^{***}p < 0.001$.

3. Results and discussion

3.1. Characterization of HA-Fc conjugates and nanoassemblies

HA-Fc and HA-Am conjugates were synthesized via amidation reaction. The ^{1}H-NMR spectra confirmed the presence of characteristic proton peaks of HA (glucoside H) and Fc-NH_2 (c) in HA-Fc, and the characteristic proton peaks of HA (glucoside H) and Am (III) in HA-Am, verified the successful synthesis of HA-Fc and HA-Am (Fig. S1). The *GD* of Fc and Am in the synthesized HA-Fc and HA-Am conjugates was 14.3 ± 1.0% and 15.3 ± 1.0%, respectively.

Particle size, zeta potential, *EE* and *DL* of the prepared nanoparticles were measured (Fig. 1A–D). The particle size of NP^3_{ST} significantly increased after being crosslinked by HA-Fc and HA-Am. The zeta potentials of nanoassemblies became more negative because of the presence of negatively charged of HA. *DL* of the HA-Fc/NP^3_{ST} utilized in this work was 1.80 ± 0.01%. Nonetheless, HA-Fc/NP^3_{ST} with a higher *DL* could be prepared by increasing the mass ratio of ST/SPC during the preparation process (Table S3). Besides, the nanoparticles showed high stability after storage for 14 days or being diluted by 50 times because negligible changes of particle size and drug leakage were observed (Fig. S2). Compared with NP^3_{ST}, both nanoassemblies showed higher stability in the presence of LCAT for even 24 h, attributing to the shield effect of HA polymers [48].

The oxidation properties of Fc were investigated. Given •OH production in the Fenton reaction triggered by the oxidation of Fc, degradation of MB after capture of •OH was utilized to characterize the H_2O_2-triggered oxidation of Fc [67]. The results showed that degradation of MB was H_2O_2 concentration-dependent and suggested that Fc was promptly oxidized by 1 mM of H_2O_2 (Fig. S3). Consequently, 1 mM of H_2O_2, a typical ROS concentration close to the oxidative stress in atherosclerotic plaque [23,54,68–71], was chosen as ROS-responsiveness condition in the following experiments in this work. FRET phenomenon was observed in Rho123-HA-Fc/NP^3_{ST}-RITC (Fig. 1E). The emission intensity of Rho123 at 524 nm decreased and that of RITC at 575 nm increased in Rho123-HA-Fc/NP^3_{ST}-RITC, indicating the energy transfer from fluorescence donor of Rho123 to acceptor of RITC and the coexistence of both components on the nanoassemblies. The FRET index was calculated as 1.768 ± 0.085, which was utilized to reflect FRET efficiency. Therefore, FRET method was utilized to confirm ROS-responsiveness of HA-Fc/NP^3_{ST}. The FRET indices of Rho123-HA-Fc/NP^3_{ST}-RITC in the presence of 1 mM of H_2O_2 significantly decreased over a course of 8 h-incubation while Rho123--HA-Am/NP^3_{ST}-RITC was unresponsive (Figs. S4A and 1F). The

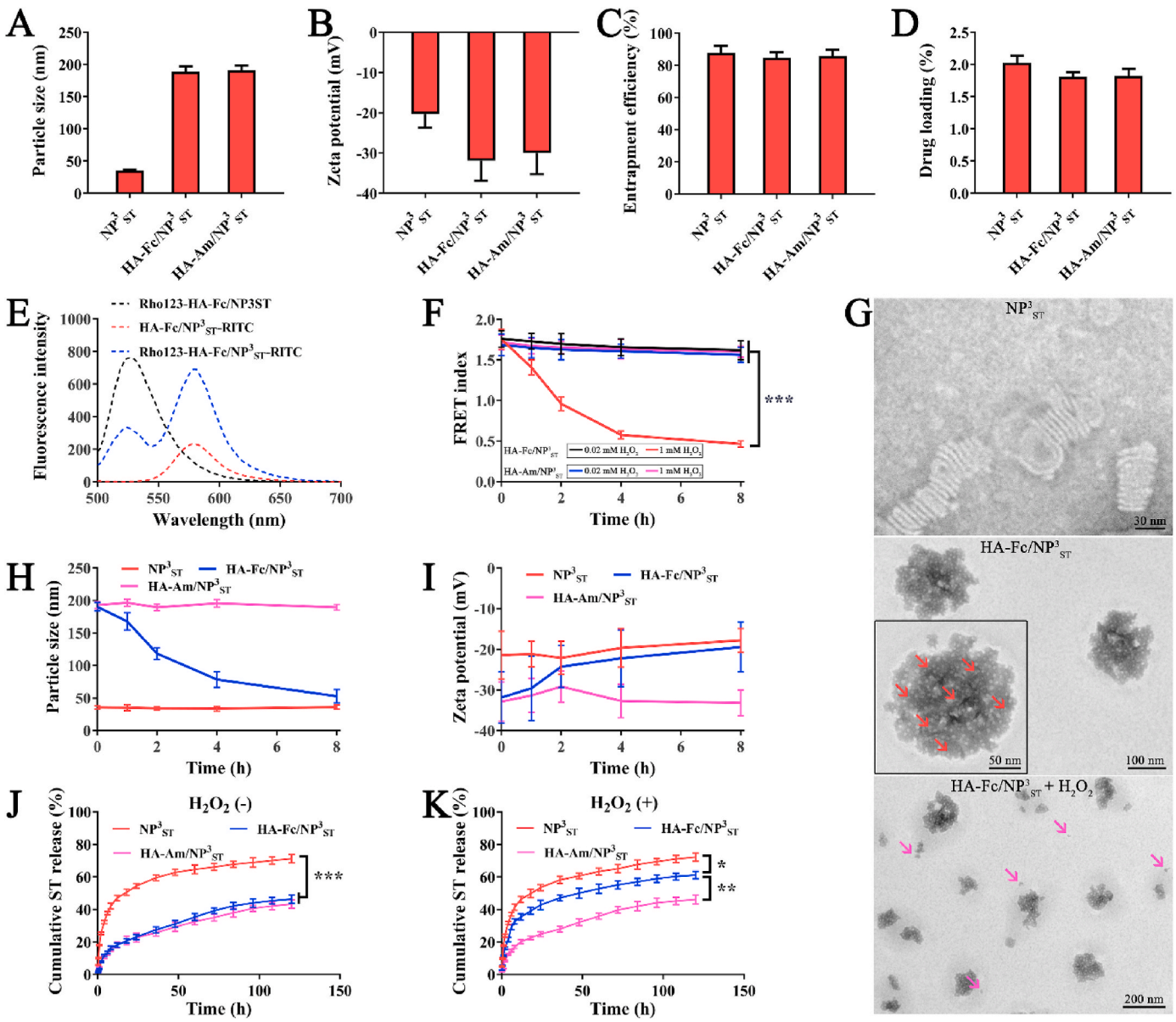

Fig. 1. Characterization of the nanoparticles. (A) Particle size (n = 5). (B) zeta potential (n = 5). (C) *EE* (n = 5). (D) *DL* (n = 5). (E) The emission spectra of Rho123-HA-Fc/NP^3_{ST}, HA-Fc/NP^3_{ST}-RITC and Rho123-HA-Fc/NP^3_{ST}-RITC with excitation at 490 nm. (F) The change of FRET indices of dual-labeled nanoassemblies during incubation with 0.02 mM or 1 mM of H_2O_2 (n = 3). (G) TEM images of nanoparticles. The red arrows indicated the discoidal particles in the TEM image of HA-Fc/NP^3_{ST}, and the purple arrows indicated the released NP^3_{ST} with small size in the TEM image of HA-Fc/NP^3_{ST} + H_2O_2. The change of particle size (H) and zeta potential (I) of nanoparticles after incubation with 1 mM of H_2O_2 (n = 5). *In vitro* drug release profiles of nanoparticles at the predetermined time points in the absence (J) and presence (K) of 1 mM of H_2O_2 (n = 5). *p < 0.05, **p < 0.01, ***p < 0.001

ROS-triggered disassembly of HA-Fc/NP^3_{ST} was visually illustrated by TEM (Fig. 1G). NP^3_{ST} exhibited as small-sized discoidal particles and aligned as rouleaux [35], which changed into large-sized spheres with multi-seed structure surrounded by a white rim after being crosslinked by HA-Fc. However, HA-Fc/NP^3_{ST} was disassembled after incubation with 1 mM of H_2O_2 for 2 h characterized by the loose and irregular shape as well as release of the small-sized particle. To directly verify the ROS-triggered size-reducible property of HA-Fc/NP^3_{ST}, the changes of particle size and zeta potential after mixing the nanoassemblies with 1 mM of H_2O_2 were measured at predetermined time points. The particle size and zeta potential of HA-Fc/NP^3_{ST} after incubation with 1 mM H_2O_2 for 8 h were close to that of NP^3_{ST} (Fig. 1H and I), which demonstrated the H_2O_2-triggered disassembly of HA-Fc/NP^3_{ST} and release of small-sized NP^3_{ST}. Furthermore, the multivalent host-guest interactions in HA-Fc/NP^3_{ST} were also verified by using FRET method (Figs. S4B and S5). FRET indices of Rho123-HA-Fc/NP^3_{ST}-RITC in the presence of 0, 1 and 5 equivs of free β-CD were almost unchanged over a course of 12 h-incubation while that promptly decreased against 50 equivs of free β-CD [72]. Subsequently, drug release in response to ROS was studied. Only 38.2% of the drug was released in 72 h in the absence of ROS (Fig. 1J), while almost 36% of drug was released within 4 h in the presence of 1 mM of H_2O_2 and 55% of drug was released after 72 h-incubation (Fig. 1K). In contrast, drug release profiles of HA-Am/NP^3_{ST} in the presence or abscence of H_2O_2 were almost no different. Taken together, we demonstrated that small-sized NP^3_{ST} were assembled into large-sized HA-Fc/NP^3_{ST} by HA-Fc conjugates based on multivalent host-guest interactions between β-CD/Fc. Upon encountering oxidative stress microenvironment mimicking the plaque intima, the hydrophobic Fc was oxidized into hydrophilic ferrocenium ion (Fc+) under the action of excess ROS, hence leading to disintegration between

β-CD/Fc, disassembly of HA-Fc/NP^3_{ST}, and release of small-sized NP^3_{ST}.

3.2. HA-Fc/NP^3_{ST} shows efficient transendothelial behavior, deeper penetration in macrophage spheroids and specific macrophage targeting ability

HA-Fc/NP^3_{ST} at the ST concentration of 5–40 μg/mL exhibited no cytotoxicity on MAECs and RAW 264.7 cells (Fig. S6). The TEER change and CD44 expression of the endothelial monolayer after TNF-α stimulation were observed (Fig. S7), suggesting the successful construction of an injured endothelium model. Drug leakage ratio of nanoparticles during the process of transendothelial transport was negligible (Fig. S8). Therefore, the measured Papp values of the drug could represent the transport behavior of nanoparticles. Besides, the TEER of the endothelial monolayer after incubation with nanoparticles for 8 h stayed almost unchanged (Table S4), indicating that endothelial monolayer was not damaged by the nanoparticles. In the transendothelial transport assessment, NP^3_{ST} exhibited the highest transendothelial capability studied in the model of continuous endothelial monolayer [73], but HA-Fc/NP^3_{ST} and HA-Am/NP^3_{ST} showed higher Papp values in the model of damaged endothelial monolayer (Fig. 2A). The pretreatment of the damaged endothelial monolayer with 10 mg/mL of free HA for 2 h [51] or 1 mg/mL of sodium azide for 1 h [74] significantly reduced transendothelial transport of HA-Fc/NP^3_{ST} and HA-Am/NP^3_{ST}. This observation suggests that the nanoassemblies crosslinked by HA polymer specifically accumulate to the damaged intercellular space and leak into the lower chamber with the help of HA-CD44 receptors affinity and that they cross the endothelial monolayer through energy-dependent transcellular transport pathway [51]. In fluorescent C6-loaded nanoparticles penetration assessment, macrophage spheroids were utilized to mimick three-dimensional structure of atherosclerotic plaque tissue and the penetration behaviors were evaluated by using CLSM (Fig. 2B and C). NP^3_{C6} showed the highest penetration ability among all the tested groups probably ascribed to its small size. ROS-responsive HA-Fc/NP^3_{C6} nanoassemblies penetrated deeper in macrophage spheroids than HA-Am/NP^3_{C6}. Nonetheless, such behavior difference in penetration was not seen in the absence of H_2O_2. The result ascertains that HA-Fc/NP^3_{C6} rapidly disassembled in response to the presence of H_2O_2 and released smaller NP^3_{C6} that penetrated deeper in the macrophage spheroids. Macrophage targeting behavior of nanoparticles was studied in the injured endothelium-macrophage monolayer model by using CLSM and flow cytometry. The C6 signal intensity increased in the following order: free C6, NP^3_{C6}, HA-Am/NP^3_{C6} and HA-Fc/NP^3_{C6} (Fig. S9, 2D and 2E). Uptake of HA-Fc/NP^3_{C6} by macrophages was significantly inhibited by the pretreatment of the endothelial cells with free HA, removal of H_2O_2 in the lower chamber or pretreatment of the macrophages with free apoA-I, suggesting that HA-Fc/NP^3_{C6} competes with free HA or apoA-I for targeting to macrophages and shows ROS-responsiveness. Cellular drug uptake profiles of nanoparticles in the macrophages of injured endothelium-macrophage monolayer model and injured endothelium-macrophage spheroid model were determined (Fig. S10). HA-Fc/NP^3_{ST} showed higher cellular drug uptake amount than either NP^3_{ST} or HA-Am/NP^3_{ST} attributing to its efficient transendothelial and macrophage spheroid penetration capacity as verified above. Taken together, HA-Fc/NP^3_{ST} shows efficient transendothelial behavior, a deeper penetration ability in macrophage spheroids and macrophage targeting *in vitro*.

3.3. HA-Fc/NP^3_{ST} exhibits effective anti-atherosclerotic effects in vitro

Cholesterol efflux from macrophages in the lower chamber of Transwell was assessed by measuring the reduction of NBD-cholesterol fluorescence intensity. Cholesterol efflux capacity increased gradually in the order: DMEM, free ST, HA-Am/NP^3_{ST}, NP^3_{ST}, HA-Fc/NP^3_{ST}. Free ST is reported to upregulate the expression of cholesterol efflux receptors on macrophage/foam cells [75], and NP^3_{ST}, the core particle, possesses favorable cholesterol removal ability [35]. HA-Fc/NP^3_{ST} showed higher cholesterol efflux capacity than free ST by 5.37-fold, NP^3_{ST} by 1.85-fold and HA-Am/NP^3_{ST} by 2.25-fold (Fig. 3A). Considering the majority of intracellular cholesterol accumulating in the cell membrane, the effect of nanoparticles on cell membrane property was evaluated. As observed, HA-Fc/NP^3_{ST} reduced cholesterol content (Fig. 3B) as well as improved permeability (Fig. 3C) and fluidity (Fig. 3D) of macrophage membrane. Oil red O staining was carried out for intracellular lipid deposition assessment. The capacity of nanoparticles to reduce intracellular lipid deposition was consistent with their cholesterol efflux capacity (Figs. 3E and S11). The changes of macrophage phenotypes were determined by flow cytometry.

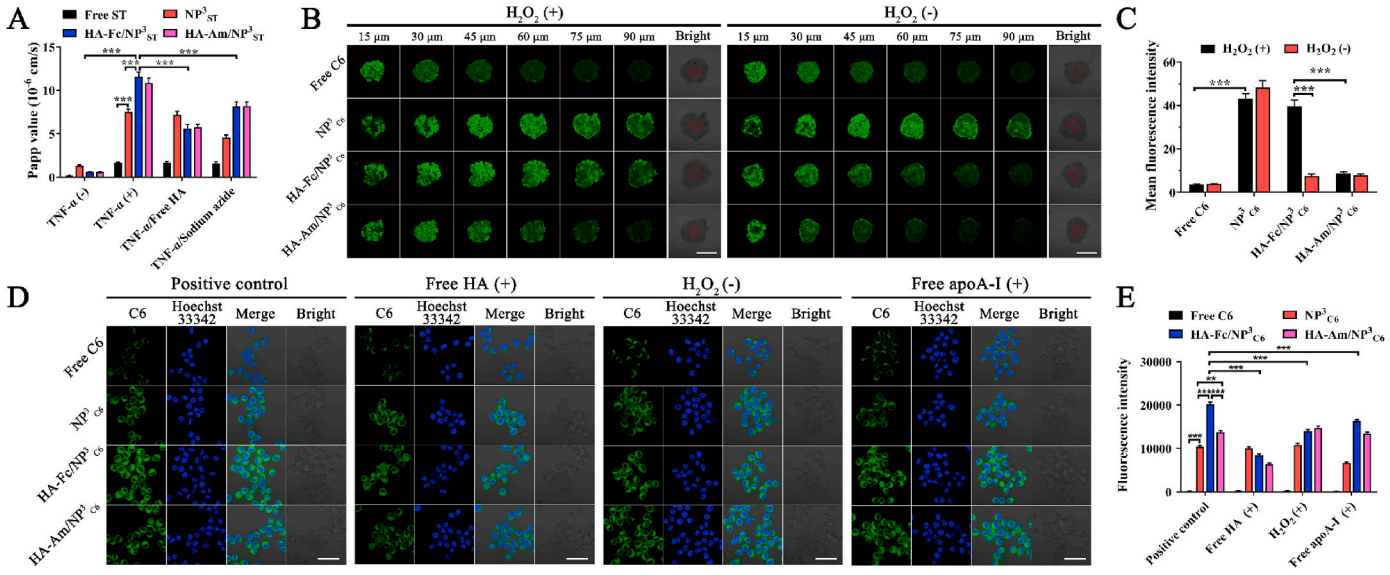

Fig. 2. Transport behaviors *in vitro*. (A) Papp values of nanoparticles across the endothelial cell monolayer (n = 5). (B) Penetration of C6-loaded nanoparticles in macrophage spheroids imaged by CLSM, and (C) quantification of fluorescence intensity in the center of spheroids at depths of 90 μm (red circles) analyzed by Image-Pro Plus 6 (n = 6). (D) Fluorescent microscopy images of the intracellular uptake of C6-loaded nanoparticles by macrophages, and (E) quantitative analysis of the cellular uptake of C6-loaded nanoparticles by macrophages after different treatments in flow cytometry study (n = 5). Scale bar: 200 μm for B, 30 μm for D; **p < 0.01, ***p < 0.001

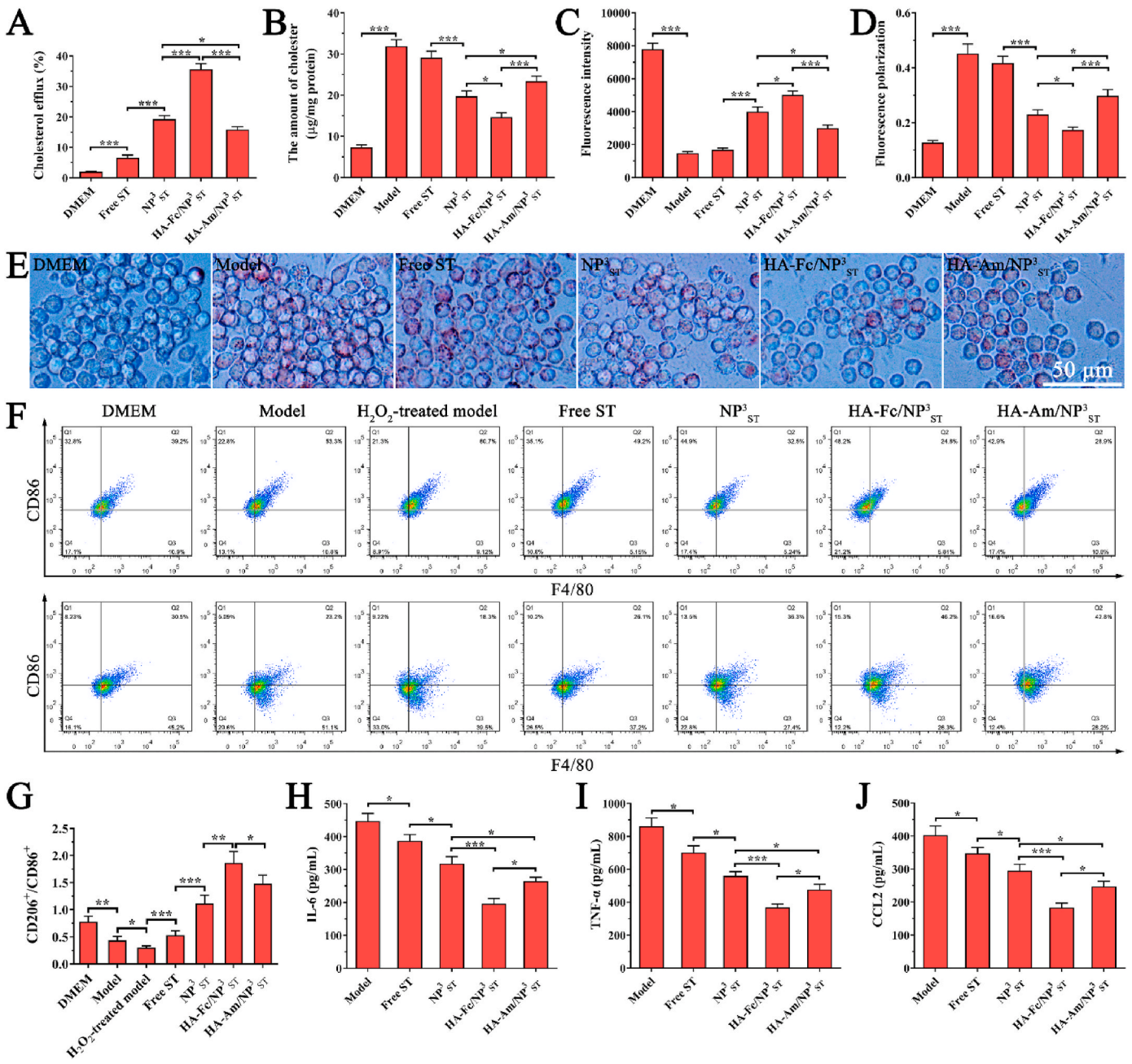

Fig. 3. Anti-atherosclerotic effects *in vitro*. (A) Cholesterol efflux (%) from macrophage-derived foam cells (n = 5). Effects of nanoparticles on the (B) cholesterol content expressed as μg/mg protein of cells, (C) permeability indicated by intracellular fluorescence intensity of fluorescent product and (D) fluidity tested by fluorescence polarization of 1,6-diphenyl-1,3,5-hexatriene (DPH) of cell membrane in macrophage-derived foam cells (n = 5). (E) Oil red O staining of intracellular lipid deposition imaged by inverted fluorescence microscope. (F) The phenotype sorting analysis of macrophages, and (G) the quantitative analysis of the M2/M1-like macrophages ratio (n = 5). Secretion levels of the inflammatory cytokines (H) IL-6, (I) TNF-α and (J) CCL2 by macrophage-derived foam cells assessed by using ELISA (n = 6). *p < 0.05, **p < 0.01, ***p < 0.001

$CD86^+/F4/80^+$ and $CD206^+/F4/80^+$ cells represented M1-like and M2-like macrophages, respectively. Both oxLDL and H_2O_2 induced the macrophages to M1 phenotype [76–79], but HA-Fc/NP^3_{ST} significantly polarized the macrophages to M2 phenotype (Fig. 3F and G), which could be explained by cellular cholesterol efflux capacity of rHDL particles [34,35] and ST intervention [80,81]. We went on to study the inhibitory effect of nanoparticles on inflammatory cytokine IL-6 (Fig. 3H), TNF-α (Fig. 3I) and CCL2 (Fig. 3J) secretion. We found that despite the stronger cholesterol efflux capacity of NP^3_{ST} than HA-Am/NP^3_{ST}, the latter was more potent in inhibiting the inflammatory cytokine secretion, presuming its higher efficiency bringing drugs to the cell. Compared with the untreated group, HA-Fc/NP^3_{ST} reduced the secretion of IL-6 by 56%, TNF-α by 57% and CCL2 by 54%.

3.4. HA-Fc/NP^3_{ST} shows improved accumulation in plaque and stronger anti-atherosclerotic effects in vivo

To verify the long circulation time of HA-based nanoassemblies, pharmacokinetics of the nanoparticles was evaluated in male wild-type C57BL/6 mice. After i.v. injection of DiR-labeled nanoparticles, DiR fluorescence intensity of blood samples colleted at a certain time interval was measured to represent the residual content of nanoparticles. Compared with free DiR or NP^3_{DiR}, fluorescence imaging indicated that HA-based nanoassemblies gained extended blood circulation (Fig. 4A

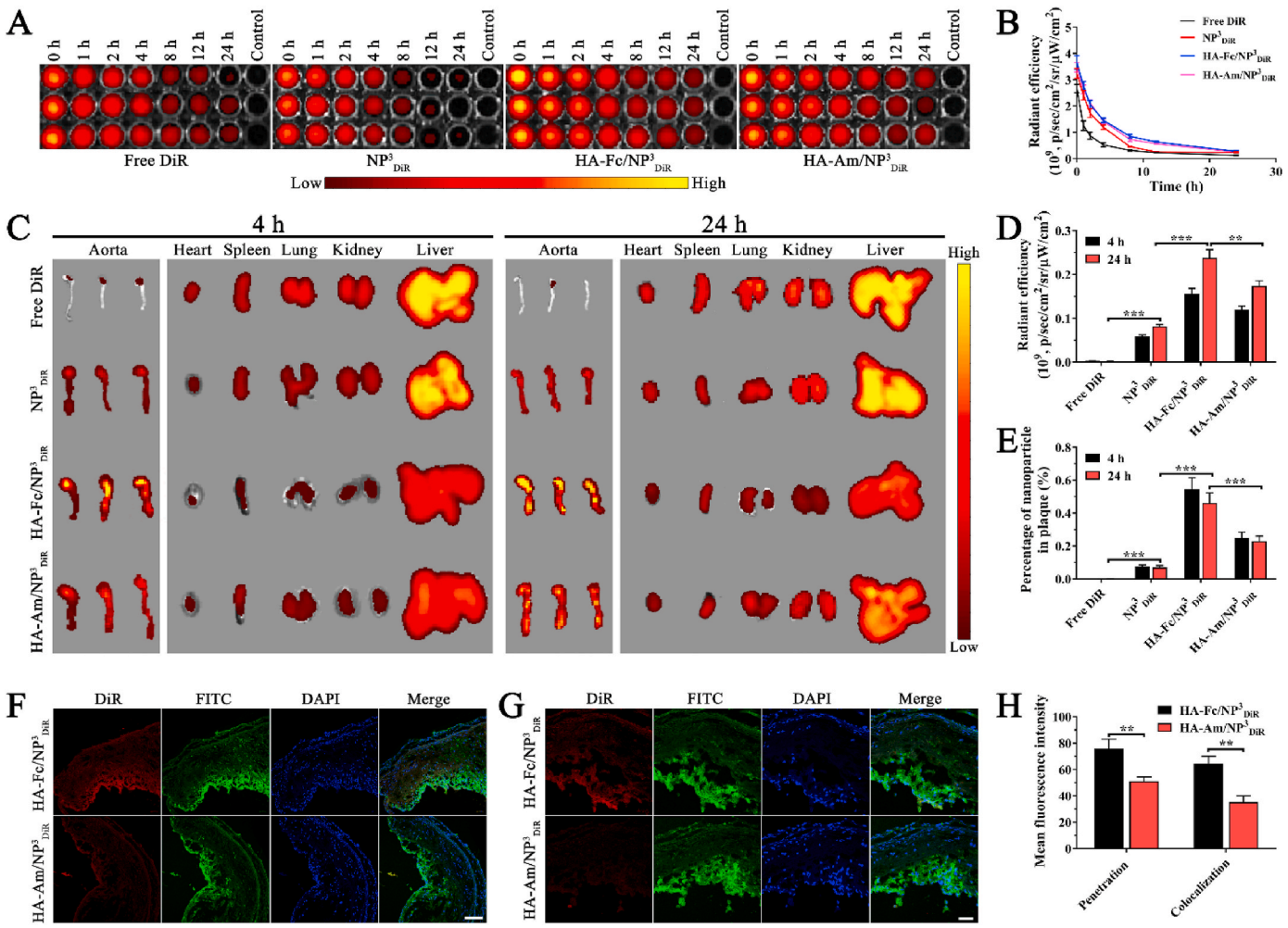

Fig. 4. Pharmacokinetic and distribution of nanoparticles in mice. (A) *Ex vivo* images, and (B) quantified DiR fluorescence intensities of whole blood collected from wild-type C57BL/6 mice at fixed time points measured by IVIS spectrum system (n = 3). (C) *Ex vivo* images of the aortas and main organs in atherosclerotic mice imaged by IVIS spectrum system, (D) quantified fluorescence intensities in the aortas and (E) the percentage of nanoparticle in plaque (n = 3). Immunofluorescence analysis of (F) the penetration ability of DiR-labeled nanoparticles (Red) across the CD31-labeled plaque tissues (Green), and (G) the colocalization of DiR-labeled nanoparticles (Red) and CD68-labeled cells (Green) imaged by CLSM, (H) quantification of DiR fluorescence intensity in the aortic root sections analyzed by Image-Pro Plus 6 (n = 3). Scale bar: 100 μm for F, 40 μm for G; **p < 0.01, ***p < 0.001

and B). Nevertheless, the majority of nanoparticles were cleared from the blood in 24 h following injection. Tissue distribution of DiR-labeled nanoparticles was also assessed in the atherosclerotic mice after i.v. injection for 4 h and 24 h (Fig. 4C–E and S12). Compared with NP^3_{DiR}, HA-based nanoassemblies showed much higher accumulation in lesion-prone aortic arch but reduced accumulations in the major organs (heart, liver, spleen, lung, kidney). The percentage of nanoparticle in plaques was calculated as the DiR fluorescence intensity in aorta/(total DiR fluorescence intensity of the main organs + DiR fluorescence intensity in aorta) × 100% [64]. HA-Fc/NP^3_{DiR} was found to accumulate in atherosclerotic lesions more efficiently than HA-Am/NP^3_{DiR}. We attributed it to the ROS-triggered disassembly and release of small-sized NP^3_{DiR} enabling deeper plaque penetration. Subsequently, distribution of the two nanoassemblies in atherosclerotic plaque was assessed. HA-Fc/NP^3_{DiR} (Red) penetrated deeply in the atherosclerotic plaque evidenced by the high fluorescence intensity in the deep of plaque tissue (CD31 labeled with green) (Fig. 4F). Meanwhile, HA-Fc/NP^3_{DiR} (Red) colocalized with the macrophages or de-differentiated vascular smooth muscle cells (VSMCs) (CD68 labeled with green) more prominently (Fig. 4G). Quantification analysis demonstrated that HA-Fc/NP^3_{DiR} penetrated deeper in atherosclerotic plaque by 1.48-fold and more effectively target to macrophages by 1.83-fold than HA-Am/NP^3_{DiR} (Fig. 4H). After that, *in vivo* anti-atherosclerotic efficacy of HA-Fc/NP^3_{ST} was confirmed more effective than either NP^3_{ST} or HA-Am/NP^3_{ST} (Fig. 5A and B). Compared with the saline group, HA-Fc/NP^3_{ST} reduced plaque size by 53%, decreased plaque lipid deposition by 63%, lowered CD68-positive cells content (macrophages or de-differentiated VSMCs) by 62% and resulted in reduction of inflammatory factor CCL2 by 64%. Meanwhile, HA-Fc/NP^3_{ST} reduced serum inflammatory factor levels of IL-6 by 52% (Fig. 5C), TNF-α by 59% (Fig. 5D) and CCL2 by 48% (Fig. 5E) than the saline group, which suggested its potent inhibitory effects on systemic inflammation. Finally, safety study was performed in atherosclerotic mice. HA-Fc/NP^3_{ST} did not cause toxicity to the liver and kidney as similar levels of ALT, AST and ALP were observed in the saline and HA-Fc/NP^3_{ST} groups (Fig. 5F). Besides, HA-Fc/NP^3_{ST} did not cause pathological damages to the major organs (Fig. 5G). Collectively, HA-Fc/NP^3_{ST} exert extended blood circulation, accumulate in atherosclerotic lesions, penetrate deeply in plaque and target to the macrophages. Moreover, HA-Fc/NP^3_{ST} exhibit effective antiatherosclerotic activity but show almost no safety problems to the atherosclerotic mice. That is to say, HA-Fc/NP^3_{ST} has potential clinical use for the treatment of atherosclerosis via alleviating inflammation and lowering lipid deposition in plaque, while its complicated preparation process can be a challenge for large scale production. Furthermore, the effectiveness and

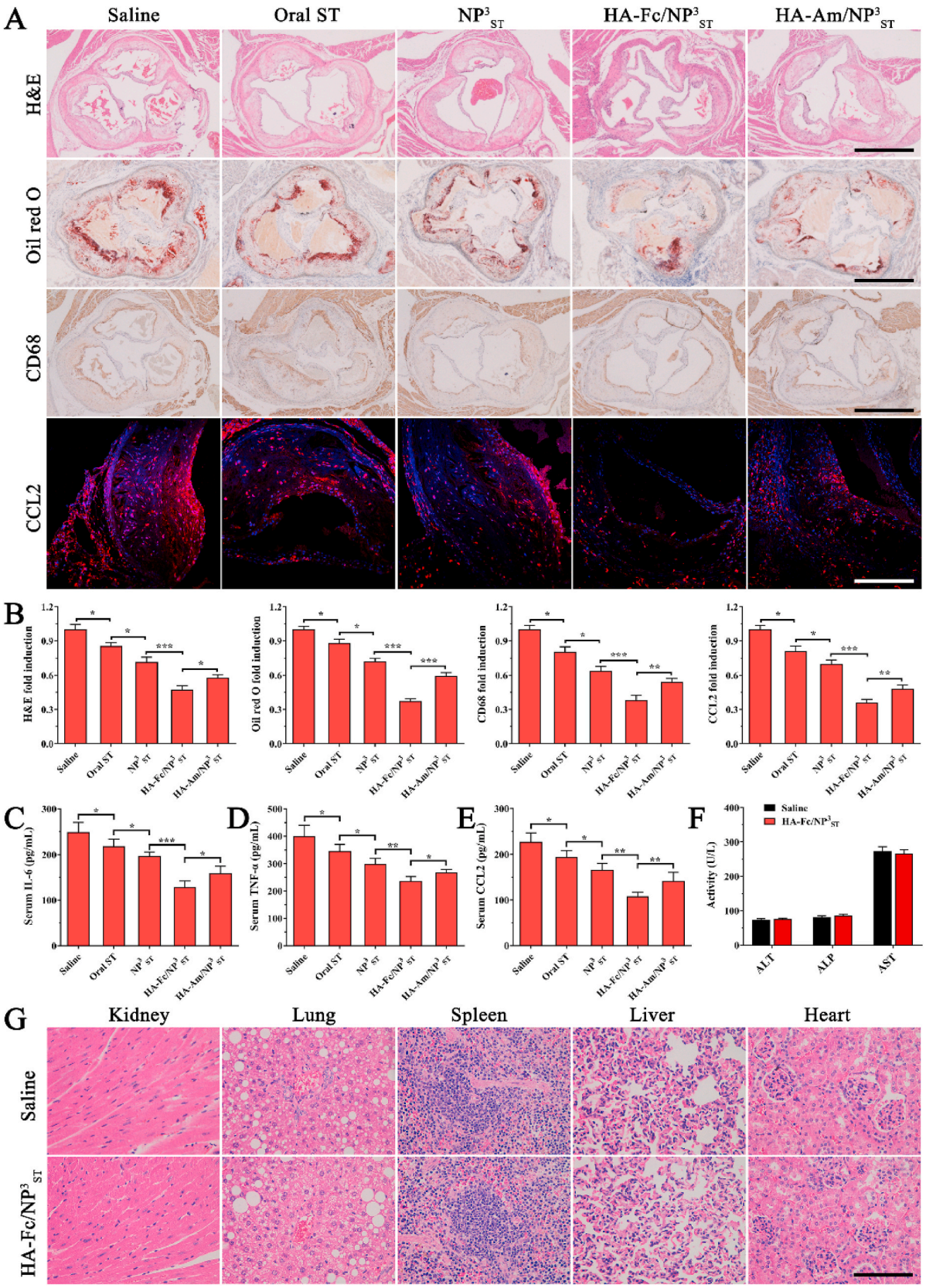

Fig. 5. Pharmacodynamics and safety studies in mice. (A) Representative images, and (B) quantitative analysis of aortic root sections stained with H&E for plaque size, oil red O staining for neutral lipid deposition, CD68 immunostaining for CD68-positive cells content and CCL2 immunostaining for inflammatory factor level in atherosclerotic mice (n = 6). The serum levels of (C) IL-6, (D) TNF-α and (E) CCL2 from the atherosclerotic mice (n = 6). (F) The activity of ALT, ALP and AST activity in plasma from the atherosclerotic mice (n = 6), and (G) H&E histopathological staining of major organs (heart, kidney, liver, spleen, lung). Scale bar: 1000 μm for H&E, oil red O and CD68 as well as 200 μm for CCL2 in A, 200 μm for G; *p < 0.05, **p < 0.01, ***p < 0.001

biosafety have been demonstrated in atherosclerotic mice only. Given that there exist obvious pathological differences between humans and mice, HA-Fc/NP^3_{ST} should be thoroughly evaluated in large animal models of atherosclerosis to better predict its efficacy and safety and then tested in clinical trials.

4. Conclusions

In this work, ROS-responsive size-reducible HA-Fc/NP^3_{ST} nanoassemblies were developed successfully for targeted atherosclerosis therapy. HA-Fc/NP^3_{ST} were assembled via multivalent host-guest interactions between β-CD/Fc with ROS-responsiveness in the atherosclerotic lesions. HA-Fc/NP^3_{ST} effectively crossed the injured endothelium via the recognition of HA-CD44 receptors, disassembled rapidly caused by ROS, penetrated deeper in macrophage spheroids and promoted macrophage-targeted cholesterol efflux. HA-Fc/NP^3_{ST} specifically accumulated in an atherosclerosis-prone region, effectively penetrated through the plaque and highly colocalized with the atherosclerotic plaque-associated macrophages. HA-Fc/NP^3_{ST} exhibited much improved antiatherogenic effects. In summary, rHDL-based ROS-responsive HA-Fc/NP^3_{ST} nanoassemblies represent a new drug delivery system for deeper penetration into atherosclerotic plaque and enhanced macrophage targeting, effectively enhancing cholesterol efflux and exerting anti-inflammatory therapy for atherosclerotic diseases.

CRediT authorship contribution statement

Jianhua He: Conceptualization, Formal analysis, Investigation, Methodology, Validation, Writing – original draft. **Wenli Zhang:** Conceptualization, Methodology, Project administration, Resources, Supervision. **Xiaoju Zhou:** Methodology, Investigation, Validation. **Fengfei Xu:** Investigation, Validation. **Jiahui Zou:** Investigation, Formal analysis. **Qiqi Zhang:** Investigation. **Yi Zhao:** Methodology, Formal analysis. **Hongliang He:** Methodology, Writing – review & editing. **Hu Yang:** Discussion, Writing – review & editing. **Jianping Liu:** Conceptualization, Funding acquisition, Project administration, Resources, Supervision, Writing – review & editing.

Declaration of competing interest

There are no conflicts of interest to declare.

Acknowledgments

This work was supported by grants from the National Natural Science Foundation of China (grant no. 81773669 and 82073788), National Major Science and Technology Projects of China (grant no. 2017YFA0205400). The authors would like to thank Xiaonan Ma and Minhui Sun at the Cellular and Molecular Biology Center of China Pharmaceutical University for their technical support.

Appendix A. Supplementary data

Supplementary data to this article can be found online at https://doi.org/10.1016/j.bioactmat.2022.03.041.

References

[1] S. Kaptoge, L. Pennells, D. De Bacquer, M.T. Cooney, M. Kavousi, G. Stevens, L. M. Riley, S. Savin, T. Khan, S. Altay, World Health Organization cardiovascular disease risk charts: revised models to estimate risk in 21 global regions, Lancet Global Health 7 (10) (2019) e1332–e1345.
[2] P. Libby, The changing landscape of atherosclerosis, Nature 592 (7855) (2021) 524–533.
[3] D. Wolf, K. Ley, Immunity and inflammation in atherosclerosis, Circ. Res. 124 (2) (2019) 315–327.
[4] K.J. Moore, I. Tabas, Macrophages in the pathogenesis of atherosclerosis, Cell 145 (3) (2011) 341–355.
[5] P. Libby, P.M. Ridker, G.R.K. Hansson, Progress and challenges in translating the biology of atherosclerosis, Nature 473 (7347) (2011) 317.
[6] T.J. Barrett, Macrophages in atherosclerosis regression, Arterioscler. Thromb. Vasc. Biol. 40 (1) (2020) 20–33.
[7] C. Weber, H. Noels, Atherosclerosis: Current pathogenesis and therapeutic options, Nat. Med. 17 (11) (2011) 1410–1422.
[8] X. Zang, M. Cheng, X. Zhang, X. Chen, Targeting macrophages using nanoparticles: a potential therapeutic strategy for atherosclerosis, J. Mater. Chem. B 9 (15) (2021) 3284–3294.
[9] C. Li, Y. Dou, Y. Chen, Y. Qi, L. Li, S. Han, T. Jin, J. Guo, J. Chen, J. Zhang, Site-specific microRNA-33 antagonism by pH-responsive nanotherapies for treatment of atherosclerosis via regulating cholesterol efflux and adaptive immunity, Adv. Funct. Mater. 30 (42) (2020) 2002131.
[10] J. Zhang, Y. Zu, C.S. Dhanasekara, J. Li, D. Wu, Z. Fan, S. Wang, Detection and treatment of atherosclerosis using nanoparticles, Wiley Interdisciplinary Reviews: Nanomedicine and Nanobiotechnology 9 (1) (2017) e1412.
[11] T. Matoba, J.-i. Koga, K. Nakano, K. Egashira, H. Tsutsui, Nanoparticle-mediated drug delivery system for atherosclerotic cardiovascular disease, J. Cardiol. 70 (3) (2017) 206–211.
[12] L. Chen, Z. Jiang, O. Akakuru, L. Yang, J. Li, S. Ma, A. Wu, Recent progress in the detection and treatment of atherosclerosis by nanoparticles, Mater. Today Chem. 17 (2020) 100280.
[13] F. Yuan, L.D. Quan, L. Cui, S.R. Goldring, D. Wang, Development of macromolecular prodrug for rheumatoid arthritis, Adv. Drug Deliv. Rev. 64 (12) (2012) 1205–1219.
[14] G. Wu, W. Wei, J. Zhang, W. Nie, L. Yuan, Y. Huang, L. Zuo, L. Huang, X. Xi, H.-Y. Xie, A self-driven bioinspired nanovehicle by leukocyte membrane-hitchhiking for early detection and treatment of atherosclerosis, Biomaterials 250 (2020) 119963.
[15] A.C. Newby, A.B. Zaltsman, Fibrous cap formation or destruction—the critical importance of vascular smooth muscle cell proliferation, migration and matrix formation, Cardiovasc. Res. 41 (2) (1999) 345–360.
[16] C.J. Martos-Rodríguez, J. Albarrán-Juárez, D. Morales-Cano, A. Caballero, D. MacGrogan, J.L. de la Pompa, L. Carramolino, J.F. Bentzon, Fibrous caps in atherosclerosis form by notch-dependent mechanisms Common to arterial media development, arteriosclerosis, thrombosis, and vascular biology, ATVBAHA 120 (2021) 315627.
[17] J. Li, W. Ke, H. Li, Z. Zha, Y. Han, Z. Ge, Endogenous stimuli-sensitive multistage polymeric micelleplex anticancer drug delivery system for efficient tumor penetration and cellular internalization, Adv. Healthcare Mater. 4 (15) (2015) 2206–2219.
[18] Z. Zhou, Y. Liu, M. Zhang, C. Li, R. Yang, J. Li, C. Qian, M. Sun, Size switchable nanoclusters fueled by extracellular ATP for promoting deep penetration and MRI-guided tumor photothermal therapy, Adv. Funct. Mater. 29 (39) (2019) 1904144.
[19] R. Taniguchi, Y. Miura, H. Koyama, T. Chida, Y. Anraku, A. Kishimura, K. Shigematsu, K. Kataoka, T. Watanabe, Adequately-sized nanocarriers allow sustained targeted drug delivery to neointimal lesions in rat arteries, Mol. Pharm. (2016) 2108.
[20] Roy Aniruddha, J. Mark, Mami Murakami Ernsting, Factors controlling the pharmacokinetics, biodistribution and intratumoral penetration of nanoparticles, J. Contr. Release Off. J. Controlled Release Soc. 172 (3) (2013) 782–794.
[21] A.J. Kattoor, N.V.K. Pothineni, D. Palagiri, J.L. Mehta, Oxidative stress in atherosclerosis, Curr. Atherosclerosis Rep. 19 (11) (2017) 1–11.
[22] X. Yang, Y. Li, Y. Li, X. Ren, X. Zhang, D. Hu, Y. Gao, Y. Xing, H. Shang, Oxidative stress-mediated atherosclerosis: mechanisms and therapies, Front. Physiol. 8 (2017) 600.
[23] U. Förstermann, N. Xia, H. Li, Roles of vascular oxidative stress and nitric oxide in the pathogenesis of atherosclerosis, Circ. Res. 120 (4) (2017) 713–735.
[24] U. Förstermann, Oxidative stress in vascular disease: Causes, defense mechanisms and potential therapies, Nat. Clin. Pract. Cardiovasc. Med. 5 (6) (2008) 338–349.
[25] Q. Xu, C. He, C. Xiao, X. Chen, Reactive oxygen species (ROS) responsive polymers for biomedical applications, Macromol. Biosci. 16 (5) (2016) 635.
[26] H. Kim, Y. Kim, I.H. Kim, K. Kim, Y. Choi, ROS-responsive activatable photosensitizing agent for imaging and photodynamic therapy of activated macrophages, Theranostics 4 (1) (2014) 1–11.
[27] S.H. Lee, M.K. Gupta, J.B. Bang, H. Bae, H.-J. Sung, Current progress in reactive oxygen species (ROS)-Responsive materials for biomedical applications, Advanced Healthcare Materials 2(6) 908-915.
[28] S. Joshi-Barr, C. de Gracia Lux, E. Mahmoud, A. Almutairi, Exploiting oxidative microenvironments in the body as triggers for drug delivery systems, Antioxidants Redox Signal. 21(5) 730-754.
[29] Y. Ochi, M. Suzuki, T. Imaoka, M. Murata, H. Nishihara, Y. Einaga, K. Yamamoto, Controlled storage of ferrocene derivatives as redox-active molecules in dendrimers, J. Am. Chem. Soc. 132(14) 5061-5069.
[30] E.R. Dionne, T. Sultana, L.L. Norman, V. Toader, A. Badia, Redox-induced ion pairing of anionic surfactants with ferrocene-terminated self-assembled monolayers: Faradaic electrochemistry and surfactant aggregation at the monolayer/liquid interface, J. Am. Chem. Soc. 135(46) 17457-17468.
[31] J. Tang, M.E. Lobatto, L. Hassing, S. Van Der Staay, S.M. Van Rijs, C. Calcagno, M. S. Braza, S. Baxter, F. Fay, B.L. Sanchez-Gaytan, Inhibiting macrophage proliferation suppresses atherosclerotic plaque inflammation, Sci. Adv. 1 (3) (2015), e1400223.
[32] K. Koushki, S.K. Shahbaz, K. Mashayekhi, M. Sadeghi, Z.D. Zayeri, M.Y. Taba, M. Banach, K. Al-Rasadi, T.P. Johnston, A. Sahebkar, Anti-inflammatory action of statins in cardiovascular disease: the role of inflammasome and toll-like receptor pathways, Clin. Rev. Allergy Immunol. 60 (2) (2021) 175–199.

[33] C.A. Argmann, J.Y. Edwards, C.G. Sawyez, C.H. O'Neil, R.A. Hegele, J.G. Pickering, M.W. Huff, Regulation of macrophage cholesterol efflux through hydroxymethylglutaryl-CoA reductase inhibition, J. Biol. Chem. 280 (23) (2005) 22212–22221.

[34] Q. Zhang, J. He, F. Xu, X. Huang, Y. Wang, W. Zhang, J. Liu, Supramolecular Copolymer Modified Statins-Loaded Discoidal rHDLs for Atherosclerotic Anti-inflammatory Therapy by Cholesterol Efflux and M2 Macrophage Polarization, Biomaterials Science, 2021.

[35] J. He, Y. Yang, X. Zhou, W. Zhang, J. Liu, A shuttle/sink model composing of β-cyclodextrin and simvastatin-loaded discoidal reconstituted high-density lipoprotein for enhanced cholesterol efflux and drug uptake in macrophage/foam cells, J. Mater. Chem. B 8 (7) (2020) 1496–1506.

[36] R. Namgung, Y.M. Lee, J. Kim, Y. Jang, B.-H. Lee, I.-S. Kim, P. Sokkar, Y.M. Rhee, A.S. Hoffman, W.J. Kim, Poly-cyclodextrin and poly-paclitaxel nano-assembly for anticancer therapy, Nat. Commun. 5 (1) (2014) 1–12.

[37] H. Jeon, J. Kim, Y.M. Lee, J. Kim, H.W. Choi, J. Lee, H. Park, Y. Kang, I.-S. Kim, B.-H. Lee, Poly-paclitaxel/cyclodextrin-SPION nano-assembly for magnetically guided drug delivery system, J. Contr. Release 231 (2016) 68–76.

[38] G.Y. Lee, J.-H. Kim, K.Y. Choi, H.Y. Yoon, K. Kim, I.C. Kwon, K. Choi, B.-H. Lee, J. H. Park, I.-S. Kim, Hyaluronic acid nanoparticles for active targeting atherosclerosis, Biomaterials 53 (2015) 341–348.

[39] L. Liu, H. He, M. Zhang, S. Zhang, W. Zhang, J. Liu, Hyaluronic acid-decorated reconstituted high density lipoprotein targeting atherosclerotic lesions, Biomaterials 35 (27) (2014) 8002–8014.

[40] X. Hou, H. Lin, X. Zhou, Z. Cheng, Y. Li, X. Liu, F. Zhao, Y. Zhu, P. Zhang, D. Chen, Novel dual ROS-sensitive and CD44 receptor targeting nanomicelles based on oligomeric hyaluronic acid for the efficient therapy of atherosclerosis, Carbohydr. Polym. 232 (2020) 115787.

[41] G. Saravanakumar, J. Kim, W.J. Kim, Reactive-oxygen-species-responsive drug delivery systems: promises and challenges, Adv. Sci. 4 (1) (2017) 1600124.

[42] Y. Na, J.S. Lee, J. Woo, S. Ahn, E. Lee, W.I. Choi, D. Sung, Reactive oxygen species (ROS)-responsive ferrocene-polymer-based nanoparticles for controlled release of drugs, J. Mater. Chem. B 8 (9) (2020) 1906–1913.

[43] W. Zhang, W. Ji, J. Jia, C. Liang, J. Liu, A simple method to extract whole apolipoproteins for the preparation of discoidal recombined high density lipoproteins as bionic nanocarriers for drug delivery, J. Pharm. Pharmaceut. Sci. 18 (2) (2015) 184–198.

[44] H. Leif, Selective extraction of lecithin:cholesterol acyltransferase (EC 2.3.1.43) from human plasma, J. Biochem. Biophys. Methods 52 (1) (2002) 63–68.

[45] R. Jin, L.M. Teixeira, P.J. Dijkstra, C. Van Blitterswijk, M. Karperien, J. Feijen, Enzymatically-crosslinked injectable hydrogels based on biomimetic dextran–hyaluronic acid conjugates for cartilage tissue engineering, Biomaterials 31 (11) (2010) 3103–3113.

[46] Y. Zhu, J. Wang, X. Li, D. Zhao, J. Sun, X. Liu, Self-assembly and emulsification of dopamine-modified hyaluronan, Carbohydr. Polym. 123 (2015) 72–79.

[47] H. He, L. Liu, H. Bai, J. Wang, Y. Zhang, W. Zhang, M. Zhang, Z. Wu, J. Liu, Arachidonic acid-modified lovastatin discoidal reconstituted high density lipoprotein markedly decreases the drug leakage during the remodeling behaviors induced by lecithin cholesterol acyltransferase, Pharmaceut. Res. 31 (7) (2014) 1689–1709.

[48] W. Zhang, H. He, J. Liu, J. Wang, S. Zhang, S. Zhang, Z. Wu, Pharmacokinetics and atherosclerotic lesions targeting effects of tanshinone IIA discoidal and spherical biomimetic high density lipoproteins, Biomaterials 34 (1) (2013) 306–319.

[49] T. Murakami, S. Michelagnoli, R. Longhi, G. Gianfranceschi, G. Franceschini, Triglycerides are major determinants of cholesterol esterification/transfer and HDL remodeling in human plasma, Arterioscler. Thromb. Vasc. Biol. 15 (11) (1995) 1819–1828.

[50] W. Zhou, W. Liu, L. Zou, W. Liu, C. Liu, R. Liang, J. Chen, Storage stability and skin permeation of vitamin C liposomes improved by pectin coating, Colloids Surf. B Biointerfaces 117 (2014) 330–337.

[51] Z. Yi, G. Hai, H. Jianhua, J. Cuiping, L. Jing, Z. Wenli, Y. Hu, L. Jianping, Co-delivery of LOX-1 siRNA and statin to endothelial cells and macrophages in the atherosclerotic lesions by a dual-targeting core-shell nanoplatform: a dual cell therapy to regress plaques, J. Contr. Release 283 (2018) 241–260.

[52] L.Q. Jiang, T.Y. Wang, T.J. Webster, H.-J. Duan, J.Y. Qiu, Z.M. Zhao, X.X. Yin, C. L. Zheng, Intracellular disposition of chitosan nanoparticles in macrophages: intracellular uptake, exocytosis, and intercellular transport, Int. J. Nanomed. 12 (2017) 6383.

[53] B. D'Autréaux, M.B. Toledano, ROS as signalling molecules: mechanisms that generate specificity in ROS homeostasis, Nat. Rev. Mol. Cell Biol. 8 (10) (2007) 813–824.

[54] C. Gao, Q. Huang, C. Liu, C.H.T. Kwong, R. Wang, Treatment of atherosclerosis by macrophage-biomimetic nanoparticles via targeted pharmacotherapy and sequestration of proinflammatory cytokines, Nat. Commun. 11 (1) (2020).

[55] B. Srinivasan, A.R. Kolli, M.B. Esch, H.E. Abaci, M.L. Shuler, J.J. Hickman, TEER measurement techniques for in vitro barrier model systems, J. Lab. Autom. 20 (2) (2015) 107–126.

[56] Y. Kim, M.E. Lobatto, T. Kawahara, B.L. Chung, A.J. Mieszawska, B.L. Sanchez-Gaytan, F. Fay, M.L. Senders, C. Calcagno, J. Becraft, Probing nanoparticle translocation across the permeable endothelium in experimental atherosclerosis, Proc. Natl. Acad. Sci. Unit. States Am. 111 (3) (2014) 1078–1083.

[57] W. Zhang, C. Li, B.C. Baguley, F. Zhou, W. Zhou, J.P. Shaw, Z. Wang, Z. Wu, J. Liu, Optimization of the formation of embedded multicellular spheroids of MCF-7 cells: how to reliably produce a biomimetic 3D model, Anal. Biochem. 515 (2016) 47–54.

[58] Y. Jin, Z. Wu, C. Wu, Y. Zi, X. Chu, J. Liu, W. Zhang, Size-adaptable and ligand (biotin)-sheddable nanocarriers equipped with avidin scavenging technology for deep tumor penetration and reduced toxicity, J. Contr. Release 320 (2020) 142–158.

[59] W. Shan, X. Zhu, M. Liu, L. Li, J. Zhong, W. Sun, Z. Zhang, Y. Huang, Overcoming the diffusion barrier of mucus and absorption barrier of epithelium by self-assembled nanoparticles for oral delivery of insulin, ACS Nano 9 (3) (2015) 2345–2356.

[60] C. Ju, R. Mo, J. Xue, L. Zhang, Z. Zhao, L. Xue, Q. Ping, C. Zhang, Sequential intra-intercellular nanoparticle delivery system for deep tumor penetration, Angew. Chem. 126 (24) (2014) 6367–6372.

[61] Y. Ding, J. Liu, Y. Zhang, X. Li, H. Ou, T. Cheng, L. Ma, Y. An, J. Liu, F. Huang, Y. Liu, L. Shi, A novel strategy based on a ligand-switchable nanoparticle delivery system for deep tumor penetration, Nanoscale Horizons 4 (2019) 658–666.

[62] C. Jiang, Y. Zhao, Y. Yang, J. He, W. Zhang, J. Liu, Evaluation of the combined effect of recombinant high-density lipoprotein carrier and the encapsulated lovastatin in RAW264.7 macrophage cells based on the median-effect principle, Mol. Pharm. 15(3) 1017-1027.

[63] J. Lu, Y. Zhao, X. Zhou, J.H. He, Y. Yang, C. Jiang, Z. Qi, W. Zhang, J. Liu, Biofunctional polymer–lipid hybrid high-density lipoprotein-mimicking nanoparticles loading anti-miR155 for combined antiatherogenic effects on macrophages, Biomacromolecules 18 (8) (2017) 2286–2295.

[64] C. Jiang, Z. Qi, W. He, Z. Li, Y. Tang, Y. Wang, Y. Huang, H. Zang, H. Yang, J. Liu, Dynamically enhancing plaque targeting via a positive feedback loop using multifunctional biomimetic nanoparticles for plaque regression, J. Contr. Release 308 (2019) 71–85.

[65] M. Liu, S. Shen, D. Wen, M. Li, T. Li, X. Chen, Z. Gu, R. Mo, Hierarchical nanoassemblies-assisted combinational delivery of cytotoxic protein and antibiotic for cancer treatment, Nano Lett. 18 (4) (2018) 2294–2303.

[66] Y. Wang, L. Li, W. Zhao, Y. Dou, H. An, H. Tao, X. Xu, Y. Jia, S. Lu, J. Zhang, Targeted therapy of atherosclerosis by a broad-spectrum reactive oxygen species scavenging nanoparticle with intrinsic anti-inflammatory activity, ACS Nano 12 (9) (2018) 8943–8960.

[67] X. Xu, Z. Zeng, J. Chen, B. Huang, Z. Guan, Y. Huang, Z. Huang, C. Zhao, Tumor-targeted supramolecular catalytic nanoreactor for synergistic chemo/chemodynamic therapy via oxidative stress amplification and cascaded Fenton reaction, Chem. Eng. J. 390 (2020) 124628.

[68] M. Mittal, M.R. Siddiqui, K. Tran, S.P. Reddy, A.B. Malik, Reactive oxygen species in inflammation and tissue injury, Antioxidants Redox Signal. 20 (7) (2014) 1126–1167.

[69] B. Ma, H. Xu, W. Zhuang, Y. Wang, G. Li, Y. Wang, ROS responsive nanoplatform with two-photon AIE imaging for atherosclerosis diagnosis and "two-pronged" therapy, Small 16 (45) (2020) 2003253.

[70] B. Ma, H. Xu, W. Zhuang, Y. Wang, G. Li, Y. Wang, Reactive oxygen species responsive theranostic nanoplatform for two-photon aggregation-induced emission imaging and therapy of acute and chronic inflammation, ACS Nano 14 (5) (2020) 5862–5873.

[71] B. Ma, H. Xu, Y. Wang, L. Yang, W. Zhuang, G. Li, Y. Wang, Biomimetic-coated nanoplatform with lipid-specific imaging and ROS responsiveness for atherosclerosis-targeted theranostics, ACS Appl. Mater. Interfaces 13 (30) (2021) 35410–35421.

[72] R. Namgung, Y. Mi Lee, J. Kim, Y. Jang, B.H. Lee, I.S. Kim, P. Sokkar, Y.M. Rhee, A. S. Hoffman, W.J. Kim, Poly-cyclodextrin and poly-paclitaxel nano-assembly for anticancer therapy, Nat. Commun. 5 (2014) 3702.

[73] C. Rhrl, H. Stangl, HDL endocytosis and resecretion, Biochim. Biophys. Acta 1831 (11) (2013) 1626–1633.

[74] P. Liu, Y. Sun, Q. Wang, Y. Sun, H. Li, Y. Duan, Intracellular trafficking and cellular uptake mechanism of mPEG-PLGA-PLL and mPEG-PLGA-PLL-Gal nanoparticles for targeted delivery to hepatomas, Biomaterials 35 (2) (2014) 760–770.

[75] J. Wong, C.M. Quinn, I.C. Gelissen, W. Jessup, A.J. Brown, The effect of statins on ABCA1 and ABCG1 expression in human macrophages is influenced by cellular cholesterol levels and extent of differentiation, Atherosclerosis 196 (1) (2008) 180–189.

[76] H.-Y. Tan, N. Wang, S. Li, M. Hong, X. Wang, Y. Feng, The Reactive Oxygen Species in Macrophage Polarization: Reflecting its Dual Role in Progression and Treatment of Human Diseases, Oxidative Medicine and Cellular Longevity 2016, 2016.

[77] F. Zhou, J. Mei, S. Yang, X. Han, H. Li, Z. Yu, H. Qiao, T. Tang, Modified ZIF-8 nanoparticles attenuate osteoarthritis by reprogramming the metabolic pathway of synovial macrophages, ACS Appl. Mater. Interfaces 12 (2) (2019) 2009–2022.

[78] S.-F. Chang, P.-Y. Chang, Y.-C. Chou, S.-C. Lu, Electronegative LDL induces M1 polarization of human macrophages through a LOX-1-dependent pathway, Inflammation 43 (4) (2020) 1524–1535.

[79] X. Wang, S. Wang, G. Yao, D. Yu, K. Chen, Q. Tong, L. Ye, C. Wu, Y. Sun, H. Li, Identification of the histone lysine demethylase KDM4A/JMJD2A as a novel epigenetic target in M1 macrophage polarization induced by oxidized LDL, Oncotarget 8 (70) (2017) 114442.

[80] A. Rezaie-Majd, T. Maca, R.A. Bucek, P. Valent, M.R. Müller, P. Husslein, A. Kashanipour, E. Minar, M. Baghestanian, Simvastatin reduces expression of cytokines interleukin-6, interleukin-8, and monocyte chemoattractant protein-1 in circulating monocytes from hypercholesterolemic patients, Arterioscler. Thromb. Vasc. Biol. 22 (7) (2002) 1194–1199.

[81] T.T. Tuomisto, H. Lumivuori, E. Kansanen, S.-K. Häkkinen, M.P. Turunen, J.V. Van Thienen, A.J. Horrevoets, A.-L. Levonen, S. Ylä-Herttuala, Simvastatin has an anti-inflammatory effect on macrophages via upregulation of an atheroprotective transcription factor, Kruppel-like factor 2, Cardiovasc. Res. 78 (1) (2008) 175–184.